

Article

Performance Analysis of PEMFC with Single-Channel and Multi-Channels on the Impact of the Geometrical Model

Masli Irwan Rosli ^{1,2}, Bee Huah Lim ^{1,*}, Edy Herianto Majlan ¹, Teuku Husaini ³, Wan Ramli Wan Daud ⁴ and Soh Fong Lim ⁵

- ¹ Fuel Cell Institute, Universiti Kebangsaan Malaysia, Bangi 43600, Selangor, Malaysia
² Department of Chemical and Process Engineering, Faculty of Engineering and Built Environment, Universiti Kebangsaan Malaysia, Bangi 43600, Selangor, Malaysia
³ Department of Green Energy, Petronas Research Sdn. Bhd. (PRSB), Bandar Baru Bangi 43650, Selangor, Malaysia
⁴ Department of Chemical Engineering, Faculty of Engineering, University of Malaya, Kuala Lumpur 50603, Kuala Lumpur, Malaysia
⁵ Faculty of Engineering, Universiti Malaysia Sarawak, Kota Samarahan 94300, Sarawak, Malaysia
* Correspondence: beehuah@ukm.edu.my

Abstract: A low-performance fuel cell significantly hinders the application and commercialization of fuel cell technology. Computational fluid dynamics modeling could predict and evaluate the performance of a proton exchange membrane fuel cell (PEMFC) with less time consumption and cost-effectiveness. PEMFC performance is influenced by the distribution of reactants, water, heat, and current density. An uneven distribution of reactants leads to the localization of current density that produces heat and water, which are the by-products of the reaction to be concentrated at the location. The simplification of model geometry can affect performance prediction. Numerical investigations are commonly validated with experimental results to validate the method's accuracy. Poor prediction of PEMFC results has not been discussed. Thus, this study aims to predict the effect of geometry modeling on fuel cell performance. Two contrasting 3D model dimensions, particularly single-channel and small-scale seven-channel models were employed. Both 3D models are correlated with a multi-channel model to assess the effect of modeling dimension on the PEMFC performance. Similar stoichiometry and channel dimensions were imposed on each model, where theoretically, the PEMFC performance should be identical. The simulation findings showed that the single-channel model produced a higher current density per cm². From the contours of water and current density, the single-channel model does not show flow distribution. Thus, this leads to a higher current density generation than the small-scale model. The prediction of PEMFC performance is not thorough for the single-channel model. Therefore, the prediction of PEMFC performance is adaptable in a small-scale or comprehensive flow field.

Keywords: PEMFC; modelling geometry; channels; performance



Citation: Rosli, M.I.; Lim, B.H.; Majlan, E.H.; Husaini, T.; Daud, W.R.W.; Lim, S.F. Performance Analysis of PEMFC with Single-Channel and Multi-Channels on the Impact of the Geometrical Model. *Energies* **2022**, *15*, 7960. <https://doi.org/10.3390/en15217960>

Academic Editors: Nicu Bizon and Antonino S. Aricò

Received: 13 September 2022

Accepted: 24 October 2022

Published: 26 October 2022

Publisher's Note: MDPI stays neutral with regard to jurisdictional claims in published maps and institutional affiliations.



Copyright: © 2022 by the authors. Licensee MDPI, Basel, Switzerland. This article is an open access article distributed under the terms and conditions of the Creative Commons Attribution (CC BY) license (<https://creativecommons.org/licenses/by/4.0/>).

1. Introduction

Global energy demand is increasing exponentially due to the growing population around the world along with economic growth, particularly in emerging market economies. The worldwide attention has been shifted to renewable energy applications to enhance energy security and reduce environmental impact [1]. Among different types of fuel cells, a proton exchange membrane fuel cell (PEMFC) is one of the promising renewable energy applications [2]. The fuel cell is typically utilized in portable automotive applications due to the advantage of quick-starting, low-temperature operation, high density, and zero pollution [3]. Continuous improvement of PEMFC efficiency to attain the desired power output for automotive applications has been carried out in the past decade. The fuel cell possesses minimal weight and cost. A low-performance PEMFC significantly

hinders the application and commercialization of fuel cell technology. The computational fluid dynamics modeling approach could predict and evaluate the performance of PEMFC with minimal time and cost-effectiveness. Over the years, researchers have continuously employed numerical methods to attain comparable predicted results with the experimental values for PEMFCs [4–6]. Numerical studies on the effect of the PEMFC flow field and manifold patterns on fluid transport [5,7–9], mass and ionic transport in the membrane electrode assembly (MEA) [10–12], and PEMFC operating parameters [13,14] affecting its performance have been widely reported to understand the phenomena in PEMFCs, which are difficult to capture and expensive to build experimentally. From the literature, two geometry modeling approaches have been applied in predicting the performance of PEMFCs. The simplest model is introduced by simplifying the model geometry, where a straight or U-shaped single channel is modeled by neglecting the flow field pattern or the overall active area of the PEMFC. This model reduces the computational time and load as a single channel and eliminates the study of flow distribution. Thus, this model is commonly adopted by researchers to investigate the fluid and ionic transport in channels and toward the MEA layer [15,16]. Researchers also used this model to study the effect of channel walls on cell performance. Zhang et al. and Perng et al. used this model to study the effect of wedge-shaped fins and baffles in a channel on PEMFC performance [17,18]. The second numerical approach for PEMFC is by adopting a complete model. This includes the overall active area and complete flow field design for PEMFC performance modeling, and the model is often seen in recent literature [19,20]. Xu et al. adopted a complete model, including a full flow field on the anode and cathode, and also MEA layers for optimizing the cathode flow field [21].

The accuracy of numerical modeling is often validated with experimental values. This is usually carried out before a researcher proceeds with the numerical investigation. Numerical model validation is reported in the early part of the results and discussion to prove the reliability of numerical works. For PEMFC modeling, an I-V curve is often used to show the average difference in percentage between numerical and experimental results. The average difference is commonly known to be low or show a coinciding and similar graph trend. Zhang et al. employed a complete model to study the effect of a rib-like flow channel on PEMFC performance [22]. Validation was carried out by establishing a complete geometrical model with dimensions according to the experiment. A 2.5% difference was reported from the validation study. Another complete geometry model validation carried out by Liao et al. showed a coinciding I-V curve of numerical and experimental results [23]. Sezgin et al. validated a numerical model using a single-channel model with a 25 cm² active area experimental prototype and reported a similar I-V curve trend but with a higher difference at lower cell voltages [24]. Liu et al. validated a U-shaped model with the experimental result of a full 71 mm × 71 mm active area [25]. It was reported that the numerical models at a current density higher than 1.2 A/cm² were not accurate enough, where an average of 24% percentage difference was significant for this validation.

Literature has shown that the geometry modeling approach affects the validation results. The average percentage differences are higher for the study adopting a single-channel model and low percentage differences are shown in the literature applying a complete geometry. To date, there is scarce literature discussing the effect of the PEMFC geometry model on the distribution of reactants, temperature, water, and performance. Thus, this paper aims to present the influence of different modeling geometries based on two contrasting 3D models, particularly single-channel and small-scale seven-channel models, by focusing on 0.6 V predicted PEMFC performance. Both 3D models are correlated with a multi-channel model [26] from a previous study evaluating the effect of modeling scale on fuel cell performance. Comparisons between the models are made in terms of reactants, water, and current density distribution.

2. Modeling and Simulation

2.1. Model Geometry

Figure 1 displays the 3D single-channel and small-scale seven-channel models developed for this study. The active areas for the single-channel and small-scale seven-channel models are 7.17 cm^2 and 1.69 cm^2 . Both 3D models have similar channel dimensions to the multi-channel model from a previous study which is $0.8 \text{ mm} \times 1 \text{ mm}$ (depth \times width). All the models in this study used a parallel flow field pattern. The active area of the multi-channel model is 393.45 cm^2 with multiple parallel channels. Table 1 shows the parameters of the models. These models have different active area geometries, and this study aims to consider the effect of different model geometries considering 3D PEMFC model geometry on the predicted performance. The single-channel model represents the simplest simulation model that only consists of a single inlet-outlet channel for the anode and cathode. It has a long channel flow with no flow distribution in the model. The second 3D model developed for this study is a small-scale seven-channel model. It has seven parallel channels for both the anode and cathode. The anode flow field has a conventional parallel flow field with a single inlet and outlet. On the cathode, it has a bend C-shaped parallel flow field with two inlets and two outlets. The model has a small active area with flow distribution being considered in the model. The multi-channel model has the largest active area with multiple flow fields, as reported in the previous literature. The model has a similar configuration as the small-scale seven-channel model. The difference between both models is the size of the active area and the channel length.

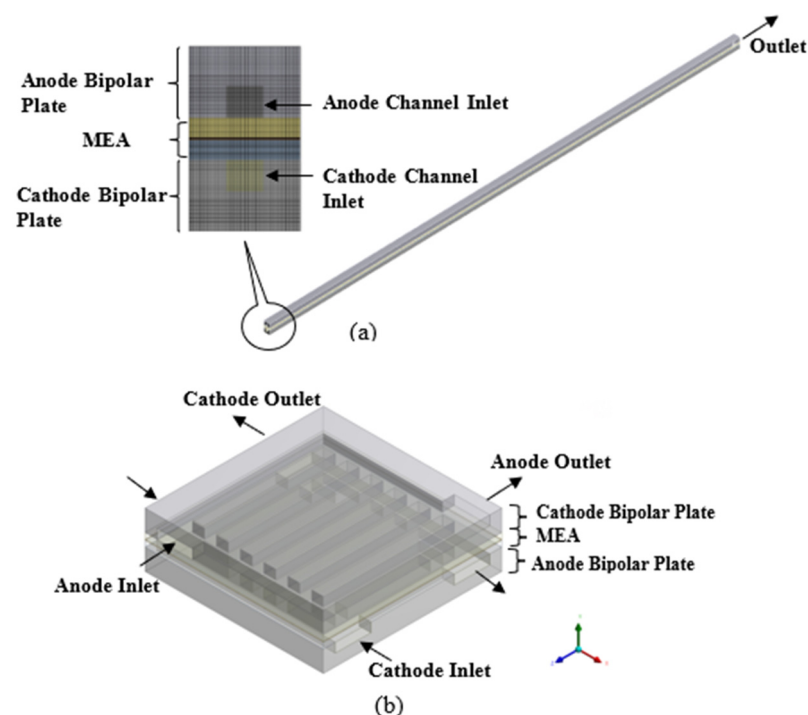
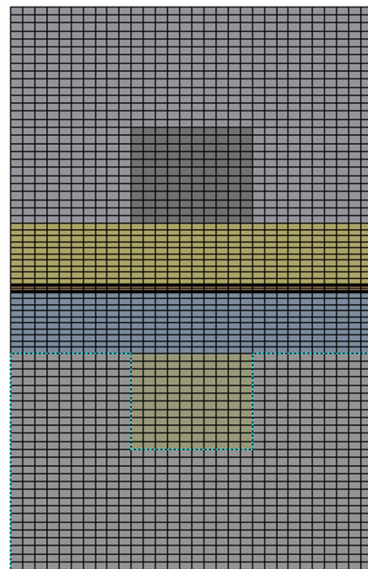


Figure 1. The 3D models: (a) single-channel model and (b) small-scale 7-channel model.

Table 1. Model Parameters.

Parameters	Value
Active area (cm ²)	7.17/1.69/393.45
Channel/Rib width (mm)	1.0
Channel Depth (mm)	0.8
Gas diffusion layer thickness (mm)	0.5
Catalyst layer thickness (mm)	0.005
Membrane thickness (mm)	0.06
Operating temperature (K)	353
Operating pressure (atm)	1.0
Hydrogen & Oxygen Stoichiometry	2

The 3D model embodies nine layers and among which five layers are the MEA with a center layer membrane. The layers are symmetrical on the anode and cathode of gas diffusion and catalyst layers. On the solid section, bipolar plates and channels create the anode and cathode compartments on the opposing sides of the bipolar plate. The PEMFC dimensions vary by no less than 5 decimal places. As a result, building a consistent mesh for the entire model is difficult. This study independently meshes each PEMFC component making it easier to capture the fluid flow and electrochemical reactions. The grid independence test (GIT) from previous work [26] was carried out to obtain the optimum grid requirement that generated approximately 3 million elements as reported. In this simulation study, the same edge sizing on all components was implemented. The single-channel and small-scale models generated 616,620 and 628,407 elements, respectively, as shown in Figure 2.

**Figure 2.** The Grid Elements of single channel model.

The boundary condition imposed on the model at the inlet was the mass flow rate. The inlet mass flow rate for both 3D models was determined using the active area with a stoichiometric value of 2. For the outlet, the outlet pressure boundary condition was imposed. The channel wall boundary condition was set as a no-slip condition. The operating pressure and temperature were set at 1 atm and 353 K, respectively.

Figure 3 shows the model validation by comparing the simulation results of the small-scale seven-channel model with the experimental results from the literature [27] using the same boundary conditions and model dimensions. The polarization curves showed a similar trend to the reference paper, indicating a reliable modeling method.

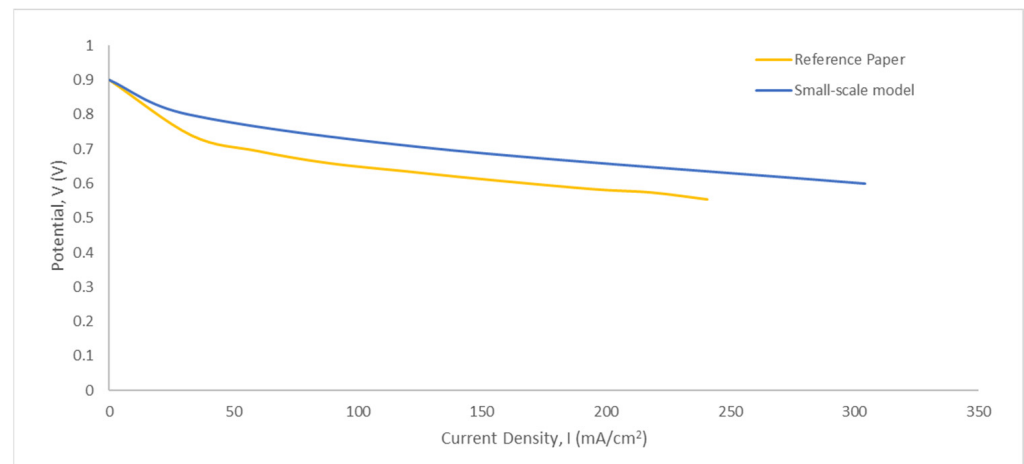


Figure 3. Polarization curve of current simulation and reference paper [27].

2.2. Numerical Method

The simulation was carried out to solve the governing equation using a commercial CFD software ANSYS Fluent with the add-on PEMFC module. The governing equations to solve the model in this study are presented in the equations below. The continuity equation is given in Equation (1).

$$\nabla(\varepsilon\rho u) = S_m \quad (1)$$

where ε represents the porosity, ρ is the density and u is the fluid velocity vector. S_m in Equation (1) has a zero in all parts of the PEMFC model except the anode and cathode catalyst layer. Equation (2) shows the momentum conservation equation where p is the pressure, μ is the viscosity, and S_u is the momentum source term.

$$\nabla \cdot (\varepsilon\rho\mu u) = -\varepsilon\nabla p + (\varepsilon\mu_{eff}\nabla u) + S_u \quad (2)$$

The energy source is represented by the changes of enthalpy, S_h in Equation (3).

$$S_h = h_{reaction} - R_{a,c}\eta_{a,c} + I^2R_{ohm} + h_{phase} \quad (3)$$

where, $h_{reaction}$ is the water heat formation, $R_{a,c}$ denotes the exchange current density of anode and cathode, I is the local current density, h_{phase} represents the enthalpy change, R_{ohm} is the ohmic resistivity of the conducting media, and $\eta_{a,c}$ denotes the overpotential in the anode or the cathode.

The transportation and formation of liquid water in cell is given in Equation (4).

$$r_w = c_r \max\left(\left[(1-s)\left(\frac{p^{wv}-p^{sat}}{RT}\right) M_{w,H_2O}\right], [-s\rho_1]\right) \quad (4)$$

where, r_w is the condensation rate, c_r denotes the condensation rate constant, l denotes liquid water and s is the saturation liquid water.

The electrochemical reaction which comprises the anodic and cathodic reactions is governed by a Butler-Volmer equation as described in Equation (5) for the anode and Equation (6) for the cathode.

$$R_a = \left(\zeta_a J_a^{ref}\right) \left(\frac{[A]}{[A]_{ref}}\right)^{\gamma_a} \left(e^{\frac{\alpha_a F \eta_a}{RT}} - e^{-\frac{\alpha_c F \eta_a}{RT}}\right) \quad (5)$$

$$R_c = \left(\zeta_c R_c^{ref}\right) \left(\frac{[C]}{[C]_{ref}}\right)^{\gamma_c} \left(-e^{\frac{\alpha_a F \eta_c}{RT}} + e^{-\frac{\alpha_c F \eta_c}{RT}}\right) \quad (6)$$

where, ζ denotes the specific active surface area, α for the transfer coefficient, γ is the concentration dependence, F for the Faraday constant, and R represents the universal gas constant.

The species transport is governed by Equation (7).

$$\nabla \cdot (\varepsilon \rho u Y_i) = \nabla \cdot (\rho D_{i,eff} \nabla Y_i) + S_i \quad (7)$$

where Y_i denotes the volume fraction species, i is the species mass fraction and $D_{i,eff}$ represent the effective species diffusivity. S_i denotes the source term of the chemical species i .

3. Results and Discussion

Three-dimensional single-channel and small-scale seven-channel models were utilized to determine the effect of geometry on the prediction of PEMFC performance. The fuel cell performance of the largest scale simulated in a previous study [26] using a multi-channel model was utilized for comparison purposes. A polarization curve was employed to determine the effect of different geometry modeling methods on PEMFC performance. Both single-channel and small-scale seven-channel models were analyzed at different cell voltages from 0.9 V to 0.4 V to predict the current density. Figure 4 shows the comparison of the polarization curves for the models developed in this study (single-channel and small-scale seven-channel models) and the multi-channel model from the previous study. The single-channel model achieved the highest performance, followed by the small-scale seven-channel model. The multi-channel model showed low performance. As reported in the previous study, the multi-channel model had the largest active area with numerous channels. The cell performance was greatly affected by the large area and a high number of channels. At a cell capacity of 0.6 V, the current density generated by the single-channel model was 0.9 A/cm², followed by the small-scale seven-channel model (0.76 A/cm²) and the multi-channel model (0.71 A/cm²).

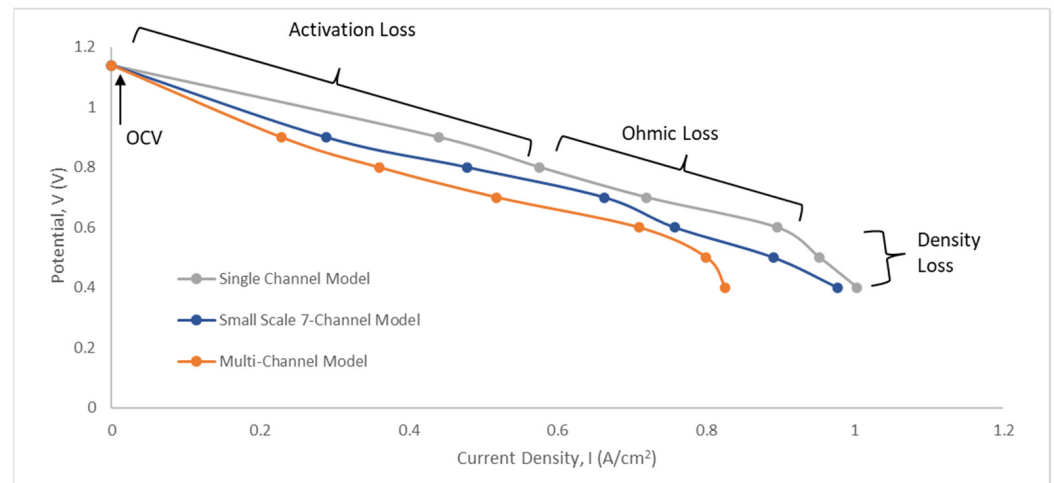


Figure 4. Polarization curves of single-channel, small-scale seven-channel, and multi-channel [26] models.

Typically, the PEMFC polarization curve is divided into three parts: activation, ohmic, and concentration losses [28]. During activation loss, the cell goes through an irreversible voltage drop in the electrochemical reaction when oxidation and reduction occur. For the single-channel model, the activation loss occurred from the open-circuit voltage (OCV) to 0.8 V. A similar activation loss from OCV to 0.9 V was observed for the small-scale seven-channel and multi-channel models because both models had a similar flow field design in which reactant distribution occurred in the models. In terms of the single-channel model, no flow distribution occurred in the simulation results. For this reason, the current density generated by the single-channel model was greater than those by the seven-channel and multi-channel models.

Ohmic losses are the center phase of a polarization curve, as depicted in Figure 4. The ohmic losses occur as a consequence of proton and electron transfer throughout the electrochemical reaction on the solid material in a particular bipolar plate, diffusion layers, and MEA. In this phase, the gradient of the graph represents the ohmic losses. The graph gradient was parallel with the ohmic loss. All three models exhibited comparable ohmic loss voltages in the range of 0.8 V-V. The multi-channel model revealed the highest ohmic loss in comparison to other models.

The final phase of the polarization curve, as illustrated in Figure 4, portrays the density loss of the material. All the models showed the occurrence of density loss after 0.6 V cell capacity. At this phase, the cell experienced reactant starvation as a result of the high current density generation. Consequently, all the models displayed a decrease in current density generation during this phase.

The single-channel model showed greater performance as a consequence of model simplification coupled with the absence of reactant distribution (Figure 4). The results from the seven-channel and multi-channel models indicated that the flow was distributed along the available channels. Figure 5a demonstrates the pressure drop between the gas diffusion layer and the channel. The comparison of the pressure drop between the anode (contour on the left) and the cathode (contour on the right) revealed that the cathode exhibited a higher pressure drop. This might be due to the entire air component (reactant) in the cathode compartment. In fact, the oxygen content in the air is only approximately 20%. Consequently, an elevated mass flow rate was dispensed to the cathode to enable the electrochemical reaction. The reactant distribution contours of hydrogen in the anode channel (contour on the left) and oxygen in the cathode channel (contour on the right) are illustrated in Figure 5b. A declining trend in reactant concentration was observed from the inlet to the outlet due to the occurrence of electrochemical reactions, where the reactants were gradually consumed along the channels [29].

Figure 5c presents the water content contour for the single-channel model in the gas diffusion layer of the anode (contour on the left) and the cathode (contour on the right). The water substance was generated during oxygen reduction. As a result, the cathode showed increasing water density on the gas diffusion layer along the flow channel. A high density of water content was evident near the inlet of the cathode. The occurrence of this phenomenon can be attributed to the higher electrochemical reaction rate near the inlet containing a high reactant concentration. The anode water distribution contour in Figure 5c indicates the presence of back diffusion in the single-channel model. Higher water content was captured near the outlet of the anode, where water permeated from the cathode to the anode due to the difference in water content [19].

Figure 6 shows the contour of current density generation with respect to the single-channel model. The current density distribution decreased from the inlet to the outlet. A similar trend was discovered in the water content distribution and reactant concentration. This phenomenon occurred because the reactants were consumed during an electrochemical reaction as water and heat were produced. A significant finding is that all three contours are interrelated. A high concentration of reactants increased the electrochemical reaction, thereby producing higher water content and current density. The single-channel model showed an even distribution of reactants from the inlet to the outlet with no flooding and a stable current density generation in the overall active area of the cell. This indicates the ideal theoretically predicted results for PEMFC generation, which shows even reactant supply and current density generation.

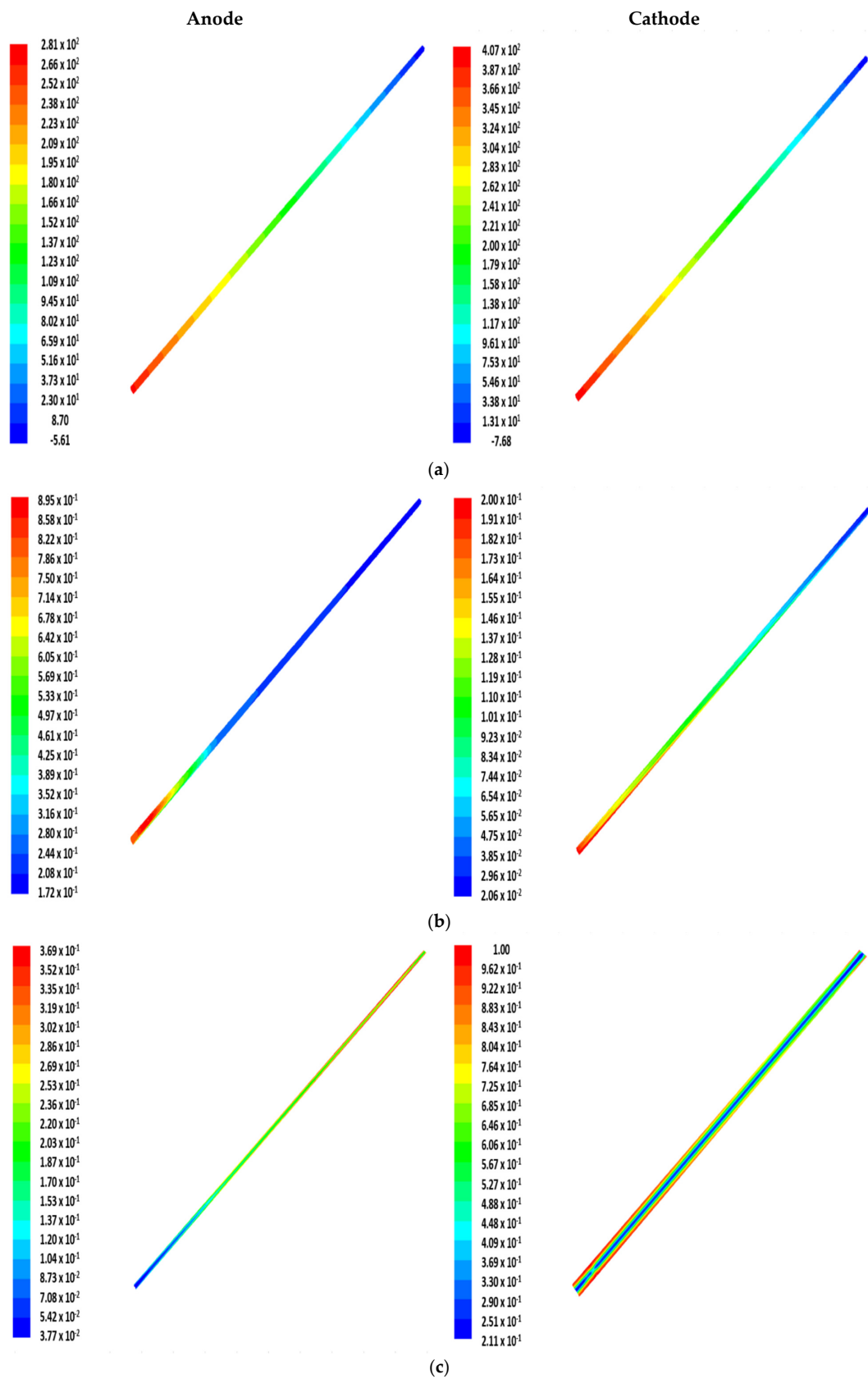


Figure 5. Contour of the single-channel model in terms of: (a) pressure distribution (Pa); (b) reactant distribution ($\text{kg}/\text{m}^3\text{s}$); and (c) water content (θ).

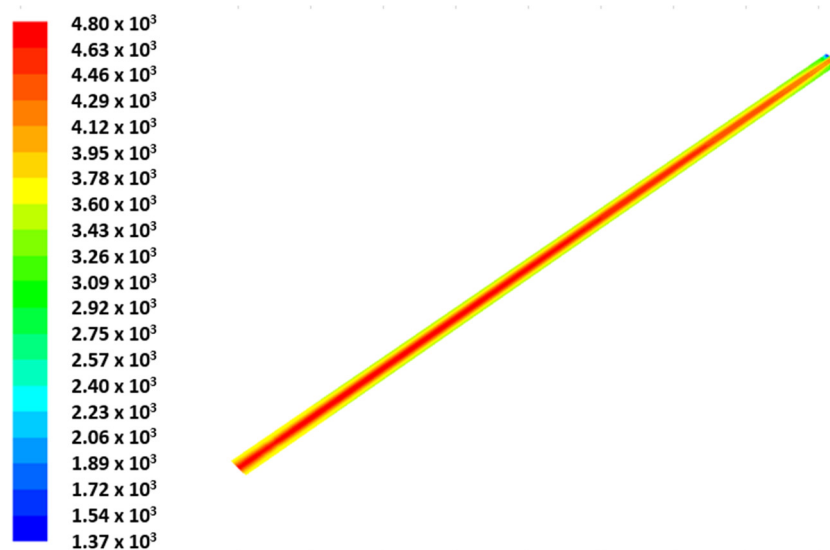


Figure 6. Current density (A/m^2) distribution contour of single-channel model.

The polarization curve in Figure 2 shows that the small-scale seven-channel model indicated lower cell performance due to the flow distribution phenomenon as compared with the single-channel model. A comparison between the small-scale seven-channel and the multi-channel model's polarization curves revealed that the former has higher cell performance. Its higher cell performance is correlated with the channel length and water flooding in the cell. A shorter channel length indicates a higher pressure drop, which affects water removal. The channel length could affect water and reactant distribution but has a low effect on current density generation [10]. Moreover, the large number of channels reduced the pressure drop and consequently reduced cell performance. Figure 7a illustrates the contour pressure distribution of the anode and cathode for the small-scale seven-channel model. A parallel flow field was used at the cathode, whereas a bend parallel flow field with a side inlet was used for the anode. A comparison between the different flow fields of the anode and cathode showed that the anode had a uniform pressure distribution with a gradually decreasing pressure from the inlet to the outlet. In contrast, the cathode had an uneven pressure distribution among the channels. The highest pressure was observed on the channels near the inlet whereas the lowest pressure occurred on the channel near the outlet. For the reactant distribution, a similar trend of distribution is displayed in Figure 7b. The result from the anode indicated a uniform distribution of reactants among the channels, whilst the cathode had an uneven distribution of reactants. The gas diffusion layer near the middle of the cathode active area had a low reactant concentration. This phenomenon can be related to the pressure distribution in which almost no pressure change occurred along the middle channels. A uniform pressure distribution in the flow channel could improve the diffusion of reactants into the gas diffusion and catalyst layers for the electrochemical reaction [30]. The hydrogen concentration on the anode gas diffusion layer decreased gradually from the inlet to the outlet. This finding proved the occurrence of an electrochemical reaction in the fuel cell. The lowest hydrogen concentration was found near the outlet on the left side of the anode. This phenomenon emerged owing to the highest oxygen concentration that existed on the cathode gas diffusion layer. Hydrogen consumption in the area was high and reached a starvation level due to insufficient hydrogen (limiting reactant) for the electrochemical reaction. On the right side of the anode, this phenomenon did not occur due to the lower oxygen concentration on the cathode gas diffusion layer. Meanwhile, on the right side of the cathode, the channel far from the inlet showed a reduction in oxygen concentration, resulting in a lower electrochemical reaction and, consequently, a lower hydrogen consumption.

Water distribution along the anode and cathode gas diffusion layers for the small-scale seven-channel model is shown in Figure 7c. As mentioned earlier, the left area of the cell had a high concentration of oxygen and hydrogen. Thus, higher electrochemical activity was expected to occur in that area, and the waste product of the reaction was a water compound. The anode gas diffusion layer showed a high water concentration near the outlet, especially on the left side, due to the occurrence of high electrochemical activity. Water accumulated on the rib area of the cathode gas diffusion layer. This result occurred due to the low-pressure drop and distribution along the channel, as well as the reduction of the purging of water from the gas diffusion layer. The contour shows the presence of liquid water in the gas diffusion layer. The theory states that a water concentration contour with a value higher than 1 indicates the presence of liquid water. In contrast, if the water concentration value is less than 1, then the water in the gas diffusion layer remains as water vapor. Figure 7c reveals that the water content with a value higher than 1 was present in the rib area, near the outlet on the anode, and the cathode gas diffusion layer. The high liquid water content in the gas diffusion layer would reduce the diffusion of reactants for electrochemical reactions in the catalyst layer [31].

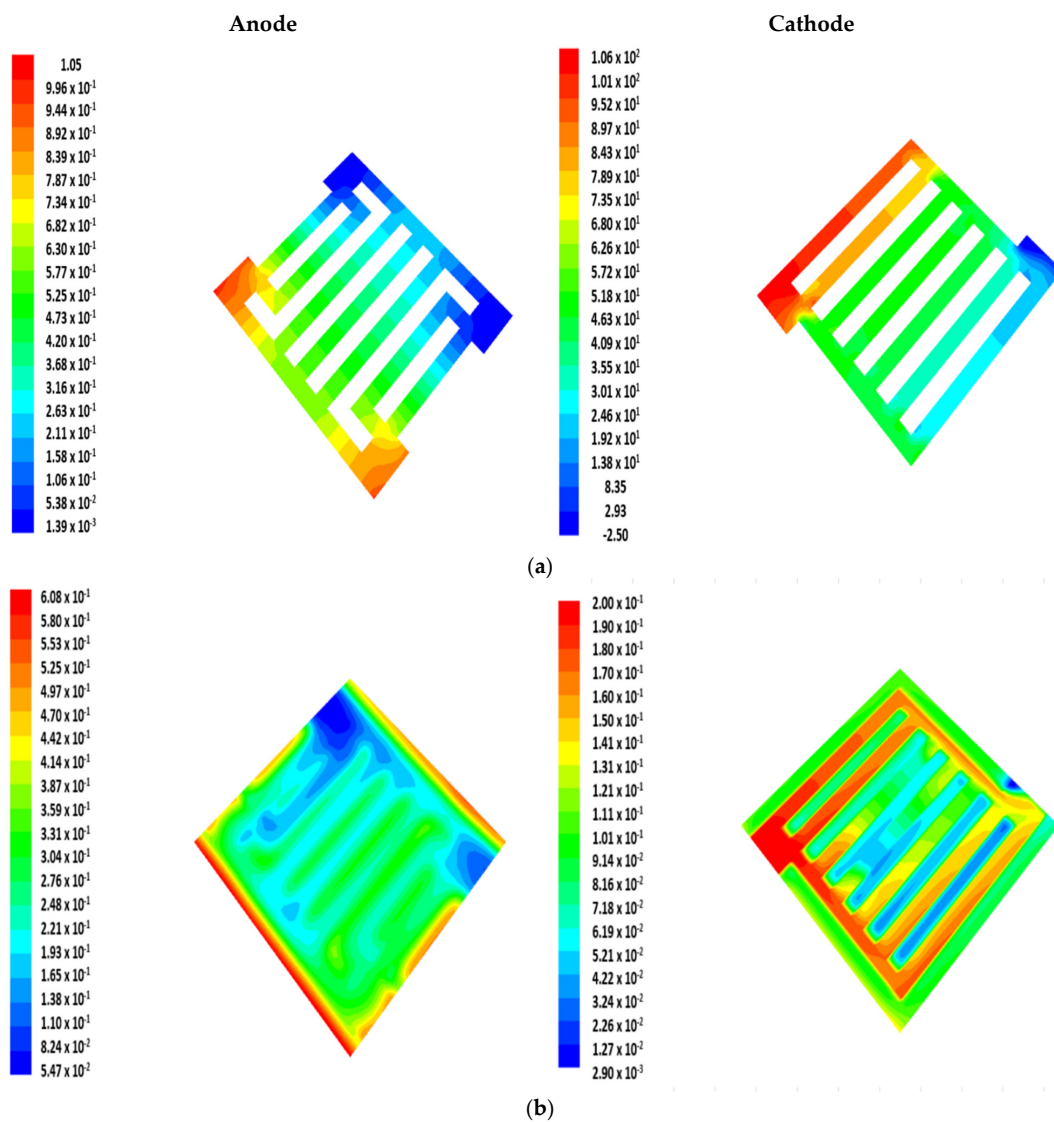


Figure 7. Cont.

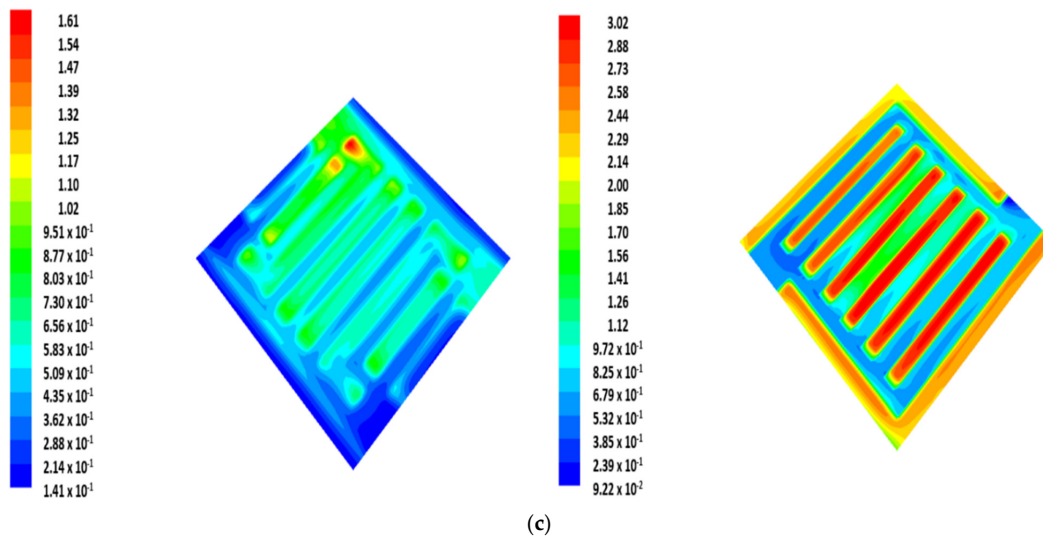


Figure 7. Contour of small-scale 7-channel model: (a) pressure distribution (Pa); (b) reactant distribution ($\text{kg}/\text{m}^3\text{s}$); and (c) water content distribution (θ).

Figure 8 displays the current density distribution on the membrane layer. The highest current density occurred along the channel area. Under the rib area, a lower current density generation occurred due to the lower diffusion of reactants, as the gas diffusion layer was occupied by liquid water. An uneven distribution of current density generation occurred due to the uneven pressure and reactant distribution. Consequently, the current density generation of the cell was lower than in the single-channel model.

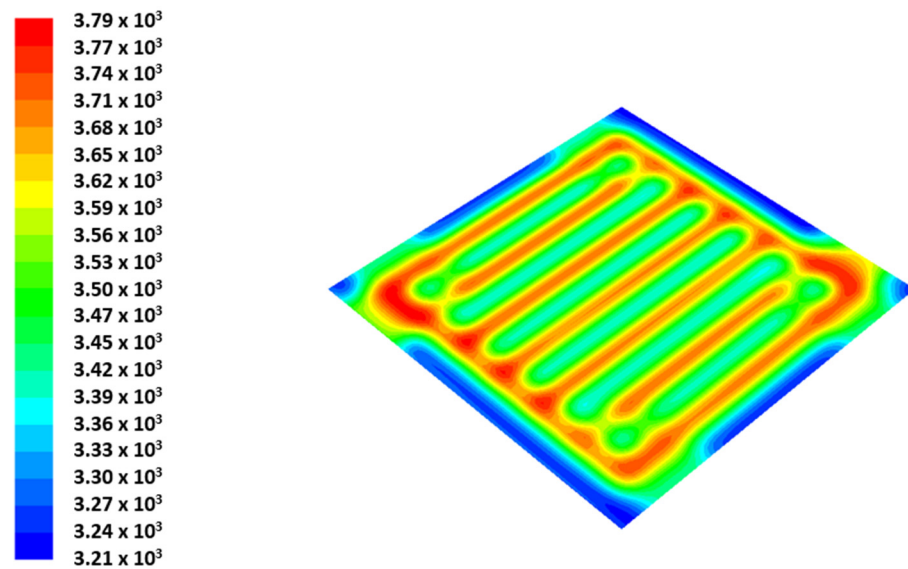


Figure 8. Current density (A/m^2) distribution contour of small-scale 7-channel Model.

The geometry model has proven to affect the PEMFC performance, as seen in Figures 6 and 8. An identical inlet stoichiometry and channel dimensions were adopted for both small-scale and single-channel models. From Figure 4, it can be seen that the current density generated per cm^2 of the active area for both models is different. As mentioned earlier, the single-channel model generated a higher current density per cm^2 than the small-scale model. Thus, the numerical model used to predict the performance of the PEMFC adapts well to the small scale or a complete flow field as compared to a simple single-channel model. This shows that a better understanding of reactants, temperature, water, and current density distribution can be obtained.

4. Conclusions

Three-dimensional single-channel and small-scale seven-channel models were developed and compared with that of a multi-channel model from a previous study to determine the effect of modeling scale on fuel cell performance. The simulation work was conducted on both 3D models. The comparison of the operating parameters (i.e., current density generation, pressure distribution, reactant distribution, and water content distribution) showed that the single-channel model had even pressure, reactant, and water content distribution from the inlet to the outlet compared with small-scale and multi-channel models. Further comparison of the performance and current density distribution showed that the multi-channel model had the lowest performance, and the distribution of current density was even throughout the active area (as reported previously) compared to the small-scale seven-channel model. This occurrence was due to the different channel lengths used. The pressure distribution in channels showed that for the small-scale seven-channel model, the cathode had a more severe reactant distribution, and flooding occurred under the rib on the gas diffusion layer. The major difference between the single-channel and small-scale seven-channel models is the flow distribution. The single-channel model does not include the flow distribution. In contrast, the small-scale seven-channel model includes the effect of flow distribution effecting the model. Both small-scale and single-channel models have the same inlet stoichiometry and channel dimensions. As indicated previously, compared to the small-scale model, the single-channel model produced a higher current density per cm^2 . In contrast to using a straightforward single-channel model, the numerical model used to estimate the performance of the PEMFC is thus found to be well adaptable to the small scale or a comprehensive flow field. Thus, a single-channel model is not encouraged for fuel cell performance prediction, because no fluid dynamic distribution occurs in the model. The major effect of fuel cell performance in the cell was the distribution of reactants and pressure, which directly affected the water and current density distribution. In conclusion, it is recommended to establish a complete flow field model for numerical prediction results of PEMFC investigation. This is beneficial to improve the performance prediction by considering the significant effect of fluid distribution in cells. To further expand the geometrical effect of numerical investigation of PEMFCs, studies on multiple cells forming a stack of PEMFC using a small-scale channel model with an expansion of dual and quad cells can be carried out in the future. Moreover, experimental work is expected to be carried out in future works to prove that the reduction in data error of a numerical model is identical to the experimental work.

Author Contributions: Conceptualization, B.H.L. and M.I.R.; methodology, B.H.L. and M.I.R.; validation, B.H.L., M.I.R. and E.H.M.; investigation, B.H.L. and M.I.R.; writing—original draft preparation, B.H.L.; visualization, B.H.L. and T.H.; supervision, E.H.M., M.I.R., T.H. and W.R.W.D.; writing—review and editing, B.H.L. and S.F.L. All authors have read and agreed to the published version of the manuscript.

Funding: This work was supported by the Ministry of Higher Education grant FRGS/1/2021/TKO/UKM/02/27.

Data Availability Statement: Not applicable.

Acknowledgments: The authors acknowledge the support from Ministry of Higher Education Malaysia for supporting this research works through research grant FRGS/1/2021/TKO/UKM/02/27 and Universiti Kebangsaan Malaysia on research opportunities.

Conflicts of Interest: The authors declare that they have no conflict of interest.

References

1. Oldenbroek, V.; Wijtzes, S.; Blok, K.; van Wijk, A.J.M. Fuel cell electric vehicles and hydrogen balancing 100 percent renewable and integrated national transportation and energy systems. *Energy Convers. Manag.* **2021**, *9*, 100077. [[CrossRef](#)]

2. Zakaria, Z.; Kamarudin, S.K.; Abd Wahid, K.A.; Abu Hassan, S.H. The progress of fuel cell for Malaysian residential consumption: Energy status and prospects to introduction as a renewable power generation system. *Renew. Sustain. Energy Rev.* **2021**, *144*, 110984. [[CrossRef](#)]
3. Lim, B.H.; Majlan, E.H.; Daud, W.R.W.; Husaini, T.; Rosli, M.I. Effects of flow field design on water management and reactant distribution in PEMFC: A review. *Ionics* **2016**, *22*, 301–316. [[CrossRef](#)]
4. Weber, A.Z.; Borup, R.L.; Darling, R.M.; Das, P.K.; Dursch, T.J.; Gu, W.; Harvey, D.; Kusoglu, A.; Litster, S.; Mench, M.M. A Critical Review of Modeling Transport Phenomena in Polymer-Electrolyte Fuel Cells. *J. Electrochem. Soc.* **2014**, *161*, F1254. [[CrossRef](#)]
5. Lim, B.H.; Majlan, E.H.; Daud, W.R.W.; Rosli, M.I.; Husaini, T. Numerical analysis of modified parallel flow field designs for fuel cells. *Int. J. Hydrogen Energy* **2017**, *42*, 9210–9218. [[CrossRef](#)]
6. Lim, B.H.; Majlan, E.H.; Daud, W.R.W.; Rosli, M.I.; Husaini, T. Three-dimensional study of stack on the performance of the proton exchange membrane fuel cell. *Energy* **2019**, *169*, 338–343. [[CrossRef](#)]
7. Rahimi-Esbo, M.; Rahgoshay, S.M.; Hassani, M.M.; Dadashi Firouzjaei, K. Novel design and numerical evaluating of a cooling flow field in PEMFC with metallic bipolar plates. *Int. J. Hydrogen Energy* **2020**. [[CrossRef](#)]
8. Liu, S.; Chen, T.; Xie, Y.; Zhang, J.; Wu, C. Numerical simulation and experimental study on the effect of symmetric and asymmetric bionic flow channels on PEMFC performance under gravity. *Int. J. Hydrogen Energy* **2019**, *44*, 29618–29630. [[CrossRef](#)]
9. Huang, F.; Qiu, D.; Lan, S.; Yi, P.; Peng, L. Performance evaluation of commercial-size proton exchange membrane fuel cell stacks considering air flow distribution in the manifold. *Energy Convers. Manag.* **2020**, *203*, 112256. [[CrossRef](#)]
10. Zhang, L.; Shi, Z. Optimization of serpentine flow field in proton-exchange membrane fuel cell under the effects of external factors. *Alex. Eng. J.* **2021**, *60*, 421–433. [[CrossRef](#)]
11. Yin, Y.; Wang, X.; Shangguan, X.; Zhang, J.; Qin, Y. Numerical investigation on the characteristics of mass transport and performance of PEMFC with baffle plates installed in the flow channel. *Int. J. Hydrogen Energy* **2018**, *43*, 8048–8062. [[CrossRef](#)]
12. Yin, B.; Xu, S.; Yang, S.; Dong, F. Influence of Microelliptical Groove Gas Diffusion Layer (GDL) on Transport Behavior of Proton Exchange Membrane Fuel Cell (PEMFC). *Int. J. Heat Mass Transf.* **2021**, *180*, 121793. [[CrossRef](#)]
13. Chen, H.; Liu, B.; Zhang, T.; Pei, P. Influencing sensitivities of critical operating parameters on PEMFC output performance and gas distribution quality under different electrical load conditions. *Appl. Energy* **2019**, *255*, 113849. [[CrossRef](#)]
14. Wang, B.; Wu, K.; Xi, F.; Xuan, J.; Xie, X.; Wang, X.; Jiao, K. Numerical analysis of operating conditions effects on PEMFC with anode recirculation. *Energy* **2019**, *173*, 844–856. [[CrossRef](#)]
15. Guo, Q.; Guo, H.; Ye, F.; Ma, C.F. Effect of liquid water accumulation in electrolytic cell mode on start-up performance of fuel cell mode of unitized regenerative fuel cells. *Energy Convers. Manag.* **2022**, *254*, 115288. [[CrossRef](#)]
16. Chen, R.; Qin, Y.; Ma, S.; Du, Q. Numerical simulation of liquid water emerging and transport in the flow channel of PEMFC using the volume of fluid method. *Int. J. Hydrogen Energy* **2020**, *45*, 29861–29873. [[CrossRef](#)]
17. Zhang, S.Y.; Qu, Z.G.; Xu, H.T.; Talkhoncheh, F.K.; Liu, S.; Gao, Q. A numerical study on the performance of PEMFC with wedge-shaped fins in the cathode channel. *Int. J. Hydrogen Energy* **2021**, *46*, 27700–27708. [[CrossRef](#)]
18. Perng, S.W.; Wu, H.W. A three-dimensional numerical investigation of trapezoid baffles effect on non-isothermal reactant transport and cell net power in a PEMFC. *Appl. Energy* **2015**, *143*, 81–95. [[CrossRef](#)]
19. Vijayakrishnan, M.K.; Palaniswamy, K.; Ramasamy, J.; Kumaresan, T.; Manoharan, K.; Rajagopal, T.K.R.; Maiyalagan, T.; Jothi, V.R.; Yi, S.-C. Numerical and experimental investigation on 25 cm² and 100 cm² PEMFC with novel sinuous flow field for effective water removal and enhanced performance. *Int. J. Hydrogen Energy* **2020**, *45*, 7848–7862. [[CrossRef](#)]
20. Tan, Q.; Lei, H.; Liu, Z. Numerical simulation analysis of the performance on the PEMFC with a new flow field designed based on constructal-theory. *Int. J. Hydrogen Energy* **2022**, *47*, 11975–11990. [[CrossRef](#)]
21. Xu, X.; Yang, W.; Zhuang, X.; Xu, B. Experimental and numerical investigation on effects of cathode flow field configurations in an air-breathing high-temperature PEMFC. *Int. J. Hydrogen Energy* **2019**, *44*, 25010–25020. [[CrossRef](#)]
22. Zhang, S.; Yang, Q.; Xu, H.; Mao, Y. Numerical investigation on the performance of PEMFC with rib-like flow channels. *Int. J. Hydrogen Energy*, 2022; in press. [[CrossRef](#)]
23. Liao, Z.; Wei, L.; Dafalla, A.M.; Guo, J.; Jiang, F. Analysis of the impact of flow field arrangement on the performance of PEMFC with zigzag-shaped channels. *Int. J. Heat Mass Transf.* **2021**, *181*, 121900. [[CrossRef](#)]
24. Sezgin, B.; Caglayan, D.G.; Devrim, Y.; Steenberg, T.; Eroglu, I. Modeling and sensitivity analysis of high temperature PEM fuel cells by using Comsol Multiphysics. *Int. J. Hydrogen Energy* **2016**, *41*, 10001–10009. [[CrossRef](#)]
25. Liu, M.; Huang, H.; Li, X.; Guo, X.; Wang, T.; Lei, H. Geometry optimization and performance analysis of a new tapered slope cathode flow field for PEMFC. *Int. J. Hydrogen Energy* **2021**, *46*, 37379–37392. [[CrossRef](#)]
26. Lim, B.H.; Majlan, E.H.; Daud, W.R.W.; Rosli, M.I.; Husaini, T. Numerical investigation of the effect of three-dimensional modified parallel flow field designs on proton exchange membrane fuel cell performance. *Chem. Eng. Sci.* **2020**, *217*, 115499. [[CrossRef](#)]
27. Macedo-Valencia, J.; Sierra, J.M.; Figueroa-Ramírez, S.J.; Díaz, S.E.; Meza, M. 3D CFD modeling of a PEM fuel cell stack. *Int. J. Hydrogen Energy* **2016**, *41*, 23425–23433. [[CrossRef](#)]
28. Barbir, F. *PEM Fuel Cells*; Academic Press: Boston, MA, USA, 2005. [[CrossRef](#)]
29. Chen, X.; Yu, Z.; Yang, C.; Chen, Y.; Jin, C.; Ding, Y.; Li, W.; Wan, Z. Performance investigation on a novel 3D wave flow channel design for PEMFC. *Int. J. Hydrogen Energy* **2021**, *46*, 11127–11139. [[CrossRef](#)]

30. Wilberforce, T.; Khatib, F.N.; Ijaodola, O.S.; Ogungbemi, E.; El-Hassan, Z.; Durrant, A.; Thompson, J.; Olabi, A.G. Numerical modelling and CFD simulation of a polymer electrolyte membrane (PEM) fuel cell flow channel using an open pore cellular foam material. *Sci. Total Environ.* **2019**, *678*, 728–740. [[CrossRef](#)]
31. Chen, X.; Chen, Y.; Liu, Q.; Xu, J.; Liu, Q.; Li, W.; Zhang, Y.; Wan, Z.; Wang, X. Performance study on a stepped flow field design for bipolar plate in PEMFC. *Energy Rep.* **2021**, *7*, 336–347. [[CrossRef](#)]